DOI: 10.1021/ma902451s

Macromolecules
ARTICLE

Layer-by-Layer Assembly of Polyelectrolytes in Nanofluidic Devices

Jonathan P. DeRocher,[†,$] Pan Mao,[‡,$] Jongyoon Han,[§,∥] Michael F. Rubner,*[,⊥] and Robert E. Cohen*[,†]

[†]*Department of Chemical Engineering,* [‡]*Department of Mechanical Engineering,* [§]*Department of Electrical Engineering and Computer Science,* [∥]*Department of Biological Engineering, and* [⊥]*Department of Materials Science and Engineering, Massachusetts Institute of Technology, 77 Massachusetts Avenue, Cambridge, Massachusetts 02139.* [$] *These authors contributed equally to this work.*

Received November 5, 2009; Revised Manuscript Received January 20, 2010

ABSTRACT: A hybrid micro-/nanofluidic device which contains an array of parallel nanochannels has been employed to study polyelectrolyte multilayer (PEM) deposition in confined geometries. Layer-by-layer (LbL) assembly of poly(allylamine hydrochloride) (PAH) and poly(styrenesulfonate) (PSS) at pH 4 and salt concentrations ranging from 0.1 to 1 M was used to conformally coat the nanochannel walls, systematically narrowing the channel width from 222 to 11 nm in the wet state. The thicknesses of confined multilayers were measured using SEM and these results were compared with those obtained on planar, unconfined surfaces. A procedure for direct measurement of the gap thickness using dc conductance was also developed. LbL assembly in the nanochannels resulted in lower bilayer thicknesses than those obtained on planar surfaces. This observation is attributed to the surface charge-induced depletion of unadsorbed polyelectrolytes within the channel. The ability to conformally coat the walls of the nanochannels with functional PEMs opens up new possibilities in the design of active nanochannel devices.

Introduction

LbL assembly has shown great utility in surface modification and functionalization, serving as a general method for assembling nanocomposite thin films made up of polyelectrolytes, nanoparticles, and biomacromolecules on a wide variety of substrates and geometries.[1] These films have been used to manipulate the optical[2−6] and wetting[2,3,7−10] properties of a surface and to impart antibacterial,[11−16] cytophilic,[17−19] magnetic,[12,20] and antifog[10,21] properties. Multilayers have also been used to achieve chemical or biological recognition and to control flow in microfluidic devices.[22]

Lithography provides a robust means of mass-producing devices with micro- and nanoscale features. Although this technique had its birth in the semiconductor industry, its utility has been well-demonstrated in the top-down fabrication of micro- and nanofluidic devices. These devices hold great potential in performing chemical and biological analyses on a very small scale, as the analytical equipment and the required sample and reagent volumes can be minimized. These devices have been utilized in technologies such as biosensing,[23,24] biomolecule separation,[25−30] and sample preconcentration.[31] Many current and potential applications depend on functionalization of the surfaces of these devices. LbL assembly provides the conformal coating necessary for surface functionalization, even for high aspect ratio nanoscale geometries, due to the self-limiting adsorption intrinsic in the process. Our aim is to combine these two robust technologies, LbL and nanofluidics, to create hybrid devices which might allow a wide range of new applications. LbL coating within nanofluidic devices provides a method of further "narrowing" nanochannels controllably, potentially down to tens of nanometers, without involving complicated fabrication methods. In addition, a wide variety of chemical functionalities available from LbL technology can be employed, while maintaining tight control of structural parameters such as pore size.

LbL assembly in confined geometries has been studied previously with two main goals: the coating of microporous or nanoporous sacrificial templates for the formation of structured materials[20,32−34] and deposition within microporous and nanoporous materials as well as microfluidic devices to impart novel functions.[22,35−43] Though the utility of multilayer deposition in confined geometries is significant, there is a lack of consensus on how confined LbL assembly differs from standard, flat substrate deposition. In particular, others have noticed discrepancies between confined and unconfined bilayer thicknesses. Although bilayer thickness can be affected by many factors such as assembly conditions and substrate or polymer chemistry, in these studies efforts were made to compare confined and unconfined deposition under the same conditions.

One example, by Lee et al., concerns the deposition of polyelectrolyte multilayers (PEMs) on porous track-etched polycarbonate (TEPC) membranes using poly(allylamine hydrochloride) (PAH) and poly(styrenesulfonate) (PSS).[35] In that work, PAH/PSS multilayers were successfully assembled within the 400 and 800 nm cylindrical pores. Bilayer thicknesses within the pores were about 20% larger than on a flat substrate, a result that was attributed to incomplete drainage of solution from the pores during the assembly process. Lee et al. also reported that as the multilayers swell within the pores, they fail to completely close the cylindrical pores; stress caused by the shrinking annular opening and electrostatic repulsion were offered as possible explanations for this observation.

Similar PEM deposition experiments on nanoporous substrates were carried out by Alem et al. using poly(vinylbenzylammonium chloride) and PSS.[44] The substrates used were TEPC membranes with pore diameters ranging from 57−845 nm. They reported

*Corresponding authors. (R.E.C.) Telephone: 617-253-3777. Fax: 617-258-8224. E-mail: recohen@mit.edu. (M.F.R.) Telephone: 617-253-4477. Fax: 617-258-7874. E-mail: rubner@mit.edu.

 Published on Web 02/10/2010

bilayer thicknesses within the pores that were 40 times higher than those on a flat substrate and attributed this result to the formation of a dense gel within the pores due to higher local polymer concentrations.

Another example of LbL polymer deposition in confinement is the tuning of photonic crystals using PAH and PSS as well as organometallic polyelectrolytes as reported by Arsenault et al.[36] The substrate used was a photonic crystal made up of close-packed, 270 nm colloidal silica microspheres. Arsenault reported five times smaller bilayer thicknesses within the crystal than on the surface of the crystal and attributed this result to exclusion, hindered diffusion, and bridging of polyelectrolyte molecules due to extreme confinement near the contact points of the colloidal particles.

Wang et al. have also reported LbL deposition of PAH and poly(acrylic acid) (PAA) in mesoporous silica particles with 3−40 nm pores to form nanoporous polymer spheres after selective dissolution of the silica template.[45,46] Thermal cross-linking of the multilayer after each deposition step was used to stabilize the polymer structure. Experiments showed that stable nanoporous polymer spheres could not be formed using porous silica particles with 2−3 nm pores, suggesting that these pores were too small to allow polyelectrolyte infiltration.

These conflicting reports comparing the bilayer thickness in confined geometries to that on flat geometries provide further motivation for systematic study of LbL deposition in structures such as micro/nanochannels. In this paper, we employ planar, essentially monodisperse rectangular channels with lateral dimensions ranging from 200 to 500 nm and depths of 10−15 μm, resulting in aspect ratios of 20−75. These channels have been developed for use in biomolecule separations and sample preconcentration[30] and provide a model experimental platform to study LbL deposition in confinement. The high throughput and high surface area in these integrated micro/nanofluidic devices combined with the ability to manipulate the chemical functionality of the device surface via LbL suggests further applications in biomolecule or chemical detection, selective separation, and heterogeneous chemical or biochemical reactions. These and other technologies will benefit from a detailed understanding of how multilayer growth within confined nanochannels compares to the well-studied case of deposition on planar surfaces.

PEMs can be used to impart a broad set of novel functionalities to a nanochannel device including stimuli-responsiveness, reversible switching of the channel gap thickness,[35] manipulation of the sign and/or the density of the surface charge, chemical functionality and wettability of the channel walls. For instance, LbL assembly has been applied to microfluidic devices as a means of controlling the surface charge of the channel walls.[22,38] Barker et al. reported that PAH/PSS multilayers could be used to create complicated electroosmotic flow patterns including flow in opposite directions in the same channel.[22] Sui and Schlenoff showed that multilayers made from PSS and a mixture of poly(diallyldimethylammonium chloride) (PDADMA) and PDADMA-*co*-PAA could be used to switch the direction of electroosmotic flow using a pH swing.[38] LbL assembly can also be used to incorporate functional nanoparticles and biomacromolecules within a surface coating, serving as a simple and general method for surface functionalization within the confined geometry of the nanochannels. Liu et al. reported LbL assembly of PDADMA and gold nanoparticles as a biocompatible, high surface area multilayer for adsorption of enzymes.[40] They coated poly(ethylene terephthalate) microchannels with this polymer/nanoparticle multilayer and immobilized trypsin on it. This catalytic microfluidic channel was found to be an efficient protein digestion device.

In this work, we use the well-studied PAH/PSS polyelectrolyte pair[47] deposited at pH 4 and different ionic strengths. PSS is a strong polyanion which is essentially fully ionized at any pH.

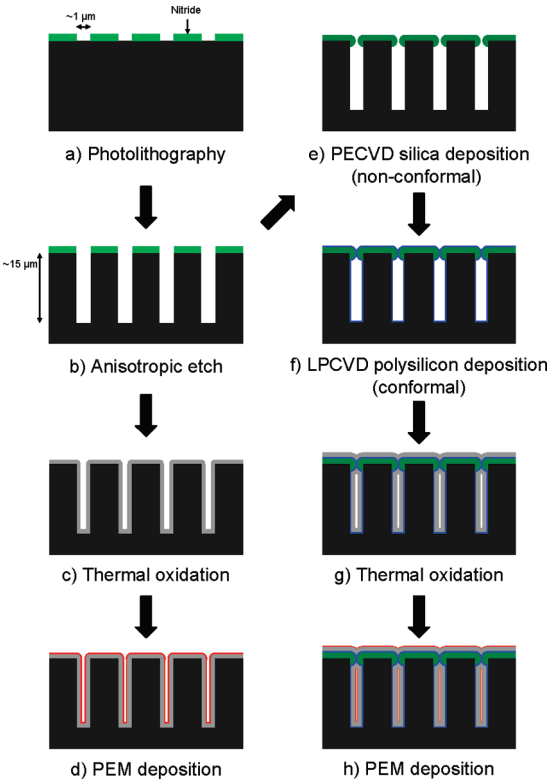

Figure 1. Schematic of the fabrication process used to form a sealed nanochannel array. Open arrays were formed by skipping the PECVD and LPCVD steps.

In contrast, PAH is a weak polycation whose degree of ionization is sensitive to pH. At pH 4, PAH is essentially fully ionized, yielding multilayers that are relatively smooth and uniform and also fairly resistant to swelling in aqueous solution. These qualities make this system a favorable one for the systematic tuning of the gap thickness in high aspect ratio channels.

Experimental Section

Materials. PAH (M_w = 56 000) and PSS (M_w = 70 000) were purchased from Sigma-Aldrich. NaCl was purchased from Mallinckrodt. Silicon wafers were obtained from WaferNet Inc. and glass slides were purchased from VWR. Poly(dimethylsiloxane) (PDMS) was made using the Sylgard 184 kit from Dow Corning. The polymer mixture was cured under vacuum at 65 °C overnight. (110) silicon wafers for nanochannel fabrication were obtained from EL-CAT Inc. Ag/AgCl electrodes were purchased from A-M Systems, Inc. and the conductivity probe and meter were obtained from VWR.

Device Fabrication. The high-aspect-ratio nanochannels were fabricated using conventional semiconductor microfabrication techniques as previously reported.[30] Two types of patterned substrates were used in this paper. One substrate consisted only of large, open nanochannel arrays for characterizing PEM growth via SEM. To fabricate this substrate, a thin layer of low-stress, low-pressure chemical vapor deposition (LPCVD) silicon nitride was deposited on a (110) silicon substrate to provide a mask for KOH etching (Figure 1a). Channel patterns were then defined by standard photolithography and etched to form narrow, deep trenches using anisotropic KOH etching (Figure 1b). The etch rate of the (110) plane in an unstirred 44 wt % KOH solution is around 75 nm/min at room temperature. After removal of the silicon nitride layer, an oxide layer with appropriate thickness was grown by thermal oxidation to narrow the gap size (trench width) to the desired value (Figure 1c).

The second device consists of a small nanochannel array bridged by microchannels to facilitate conductance measurements. In order

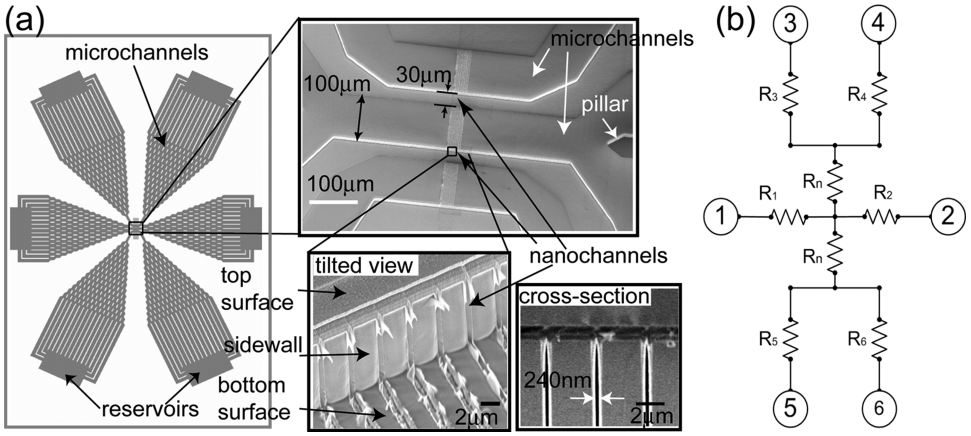

Figure 2. (a) Schematic and SEM images of the device used for the dc conductance measurements. The device consists of a nanochannel array which bridges a series of microchannels. The pyramid-shaped microchannels are used to ensure low resistance relative to the nanochannels and the pillars are required to prevent the channels from collapsing. The interface between the nanochannels and microchannels is shown in tilted-view and cross-sectional SEM images. The nanochannel is 30 μm long and 240 nm wide. The width of the microchannels is 100 μm. All channels have a depth of 15 μm. The trenches in the bottom surface near the nanochannel array are due to the overetching of the nanochannel array pattern during subsequent etching of the microchannels. (b) Simplified equivalent circuit of the device employing the assumption of ideal, inert channels.

to create both nanochannels and microchannels, a modified fabrication approach was used as described previously.[30] After photopatterning and KOH etching of deep trenches as above, plasma-enhanced chemical vapor deposition (PECVD) oxide (Figure 1e) and LPCVD polysilicon (Figure 1f) were sequentially deposited on the trenches. The combination of the nonconformal PECVD and conformal LPCVD processes allows us to maintain a uniform gap size along the trench after deposition while sealing the trenches completely. After the nanochannel array was sealed, microchannels were defined by standard photolithography and etched to the same depth as the nanochannel array using deep reactive ion etching (DRIE). Finally, thermal oxidation was used to narrow the gap size within the nanochannels to the desired initial value for the LbL coating experiments (Figure 1g). All silicon surfaces were passivated with oxide to form an insulation layer, needed for the conductance measurements. This fabrication method eliminates the rounded shape resulting from oxidation of the silicon posts and ensures a uniform gap size along the nanochannels. The device layout is shown in Figure 2a.

In order to form closed microchannels, a bonding protocol was developed to cap the channels after PEM deposition. As reported previously, O_2 plasma can be used to selectively etch a PEM film from an exterior surface, while leaving the same coating intact within small pores.[20] We removed the exposed PEM, which was covering the bonding surface, while leaving the coating inside the nanochannels intact. We found that 30 s of O_2 plasma etching (100 mTorr, 100 W) per bilayer of PAH/PSS deposited is sufficient to remove the PEM film on the top surface while leaving the film inside the nanochannels intact. A slab of PDMS (with prepunched holes corresponding to the device reservoirs) and the plasma-cleaned device were subjected to O_2 plasma for 1 min, and then aligned and brought into contact. The bonded device was then placed on a hot plate at ~90 °C for a few hours to increase the bonding strength.

PEM Deposition. For experimental convenience, silicon devices were mounted on glass slides by bonding the unpatterned side of the device with the glass substrate using double-sided tape (468MP, 3M). Polyelectrolyte solutions consisting of 10 mM polyelectrolyte (on a repeat unit basis) and salt concentrations ranging from 0 to 1 M were prepared using deionized (DI) water (18 MΩ·cm, Millipore) and adjusted to pH 4.0 using 1.0 M HCl (Sigma-Aldrich). The pH of the rinsewater was also adjusted to match that of the polyelectrolyte solutions in order to avoid pH drift over the course of an experiment. Both polymer and rinse solutions were filtered using 0.2 μm polyether sulfone filtration membranes (VWR). The samples were dipped into baths containing either polyelectrolyte or rinse solutions using a programmable slide stainer (Zeiss, Inc.). The substrates were first dipped into the polycation (PAH) solution, followed by dipping into three rinse baths. The substrate was then dipped into the polyanion (PSS) solution followed by three rinses. This process, which constitutes the assembly of one bilayer, was then repeated to form the PEM. The dip times for the polycation/polyanion and three rinse baths were 40, 10, 10, and 10 min, respectively. Upon completion of PEM deposition, the samples were immediately dried with compressed air.

Characterization. The thickness and conformality of PEM films assembled within the nanochannels were determined using scanning electron microscopy (SEM) (JEOL 6320, Zeiss Supra-40). The SEM samples were prepared by fracture of the coated silicon substrates using a diamond scorer. The dry film thicknesses of PEMs coating the open nanochannel geometry were measured using image analysis tools built into the SEM software. The micrographs were also used to qualitatively evaluate the roughness and conformality of the polymer coating.

The thickness of a PEM on a flat silicon substrate in equilibrium with a particular aqueous solution was determined using *in situ* spectroscopic ellipsometry (XLS-100, J.A. Woollam Co., Inc.). In these experiments, the sample was placed in a custom-made quartz cell[2] which was filled with the solution of interest. The resulting data were fit to a Cauchy model to determine the wet state film thickness.[47] Spectroscopic ellipsometry was also used to determine the dry PEM thickness on flat silicon substrates. Profilometry (P-16+, KLA-Tencor) was also performed on a number of flat substrate samples in the dry state. The dry state thickness values obtained from profilometry were systematically lower than those for ellipsometry, but were generally within 2% of the ellipsometry results. The wet state (1 M KCl) thicknesses on flat substrates were about 26% larger than the corresponding dry state values (see Figure S1 in the Supporting Information).

Dc Conductance Measurement. The dc conductance measurements were used to determine the ionic flux through the channels, from which estimates of the gap thickness could be made. These experiments were performed using a Keithley 236 source/measurement unit. Before measuring the electrical conductance of a device, it was first soaked in a solution of 1 M KCl overnight. The device was flushed with fresh KCl solution and allowed to stand for a few minutes to allow the liquid level in each reservoir to equilibrate. This was done to prevent convection from affecting the conductance measurements. The device was connected to the voltage source by two Ag/AgCl electrodes

placed into two specified reservoirs. Ag/AgCl electrodes were used to prevent overpotential during the measurement. A low voltage sweep from −0.5 to +0.5 V was performed at a rate of 0.01 V/s. The Keithley 236 was controlled using a custom-made LabView 7.0 program. The dc conductances of channels were determined by fitting the slope of the ionic current as a function of the applied voltage ($I-V$ plot). These plots always showed very linear behavior, with R^2 values of at least 0.99, confirming that we have an ohmic system (see Figure S2 in the Supporting Information for a representative plot).

The nanochannel conductance S_n can be written as:[48]

$$S_n = \frac{1}{R_n} = (\mu_{K^+} + \mu_{Cl^-})\left(n_{KCl}e\frac{W_nH_n}{L_n} + \sigma_s\frac{H_n}{L_n}\right) \quad (1)$$

where R_n is the resistance, μ_i is the mobility of species i, n_{KCl} is the concentration of KCl, e is the elementary charge, σ_s is the surface charge density, and W_n, H_n, and L_n are the dimensions of the nanochannel (see Figure S3 in the Supporting Information). At high salt concentrations (for example 1 M KCl), where $W_n \gg \lambda_D$ (Debye length) and $|\sigma_s| \ll en_{KCl}W_n$ we can ignore the second term, which is governed by surface charge, and assume idealized, inert channel behavior, modeled as ideal resistors.[49] The equivalent channel circuit of the device is shown in Figure 2b.

To determine the conductance of the nanochannels, one must first account for the resistance of the microchannels which connect the reservoirs to the nanochannel array. For the circuit between reservoirs 1 and 2 we know that

$$R_{12} = R_1 + R_2 \quad (2)$$

where R_{ij} is the resistance between reservoirs i and j. Similarly, between 3 and 4, we have

$$R_{34} = R_3 + R_4 \quad (3)$$

For the circuits which include the nanochannels, we have:

$$R_{13} = R_1 + R_3 + R_n \quad (4)$$

$$R_{24} = R_2 + R_4 + R_n \quad (5)$$

where R_n is the resistance of the nanochannel array. Solving for R_n we can write:

$$R_n = \frac{R_{13} + R_{24} - R_{12} - R_{34}}{2} \quad (6)$$

The resistance of an array of cuboid nanochannels is given by

$$R_n = \frac{\rho L_n}{NH_nW_n} \quad (7)$$

where ρ is the resistivity of the electrolyte (KCl) solution and N is the number of nanochannels in the array. Solving for the channel width (W_n) gives:

$$W_n = \frac{2\rho L_n}{NH_n(R_{13} + R_{24} - R_{12} - R_{34})} \quad (8)$$

Here R_{13}, R_{24}, R_{12}, and R_{34} are experimentally determined from the inverse of the slope of the $I-V$ plot for each case. For the devices used in this paper, $N = 10$, $L_n = 30\ \mu$m, and $H_n = 15\ \mu$m. The conductivities ($1/\rho$) of 200 mM, 1 M, and 3 M KCl solutions were measured using a conductivity probe (VWR) and found to be 25.01, 113.8, and 290.1 mS/cm, respectively. From the gap size (width, W_n) of a nanochannel, we can obtain the film thickness (d) inside the nanochannel, which is:

$$d = (W_0 - W_n)/2 \quad (9)$$

where W_0 is the gap size of the nanochannel before PEM coating. Here we assume that the ionic transport inside the hydrated multilayer is negligible compared to the ionic flux through the open portion of the nanochannel. This assumption is justified[50] since hydrated PEMs have conductivities of order 10^{-9} S/cm while our KCl electrolyte solutions have significantly higher conductivities of order 10^{-1} S/cm.

Results and Discussion

Polymer Coil Dimensions. An important consideration for deposition of polymer molecules within a nanofluidic channel is the size of the polymer coil in solution. One means of characterizing coil dimensions is the mean square end-to-end distance, given by:

$$\bar{r}^2 = \alpha^2 C_\infty n\boldsymbol{l}^2 \quad (10)$$

where α is the coil expansion factor, C_∞ is the characteristic ratio, n is the number of bonds, and $\boldsymbol{l}$ is the bond length. The upper bound for this quantity is the contour length, which is 150 nm for PAH and 85 nm for PSS. In contrast, the lower bound for this quantity is the unperturbed chain length for which $\alpha = 1$ (theta conditions). Using a characteristic ratio of 7.8[51] for PSS, the unperturbed root-mean-square (rms) end-to-end distance is about 11 nm. Using a characteristic ratio of 6.6 from poly(1-butene)[52] for PAH, the unperturbed dimensions are 14 nm. For polyelectrolytes, the charged nature of the backbone leads to coil expansion due to long-range electrostatic repulsion. The ionic strength therefore affects coil dimensions by screening these repulsive interactions. Borochov and Eisenberg measured the radius of gyration of 10^6 g/mol PSS at different salt concentrations and found that the radius of gyration was 51 nm at 0.1 M NaCl and 108 nm at 10^{-3} M NaCl.[53] These values correspond to rms end-to-end distances of 33 nm at 0.1 M and 70 nm at 10^{-3} M for our lower molecular weight PSS. If we use the coil expansion factors implied by these values to estimate the dimensions for PAH coils, we find that the rms end-to-end distances are approximately 40 nm at 0.1 M and 85 nm at 10^{-3} M.

Polyelectrolyte Multilayer Growth in Nanochannels. The assembly of PAH/PSS multilayers in open nanochannel arrays was investigated using SEM. Figure 3 is a cross-sectional view of a nanochannel array that was successfully coated with 40 bilayers of PAH/PSS at pH 4.0 and 0.1 M NaCl. The SEM image shows that good coating uniformity was achieved along the length of multiple channels. We found the quality of the coating to be sensitive to the deposition conditions. Optimal coatings were obtained when depositions were performed with pH-adjusted rinse solutions and the sample was not allowed to dry until deposition was complete. We also have evidence that surface treatment may play a part in improving the uniformity of the coating. In particular, we have found that preassembly sonication of the nanochannel array in surfactant (3% Micro-90, International Products Corp.) and acid solutions (1 M HCl) tends to give more uniform films. To further quantify the coating uniformity, SEM micrographs of various regions of coated nanochannel arrays were analyzed to determine the PEM thickness. Samples coated with various numbers of bilayers of PAH/PSS assembled at pH 4.0 and 0.1 M NaCl were used to perform this analysis. The results are summarized in

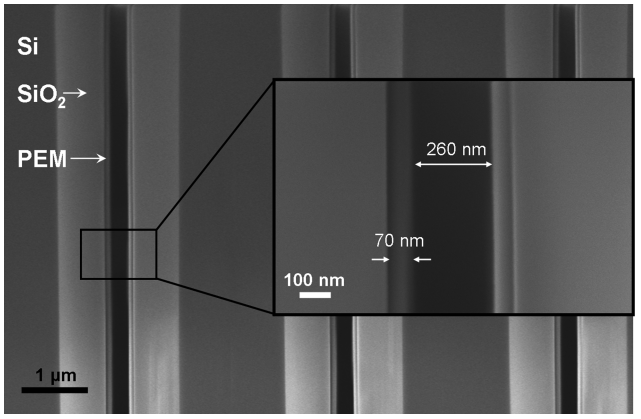

Figure 3. Scanning electron micrographs depicting conformal coating of an open nanochannel array with a 40 bilayer PEM of PAH/PSS deposited at pH 4.0 with 0.1 M added NaCl. The silicon, thermally grown oxide layer, and PEM are clearly visible. The inset shows that the 400 nm channels have been reduced to a gap size of 260 nm by the LbL deposition of a 70 nm thick PEM.

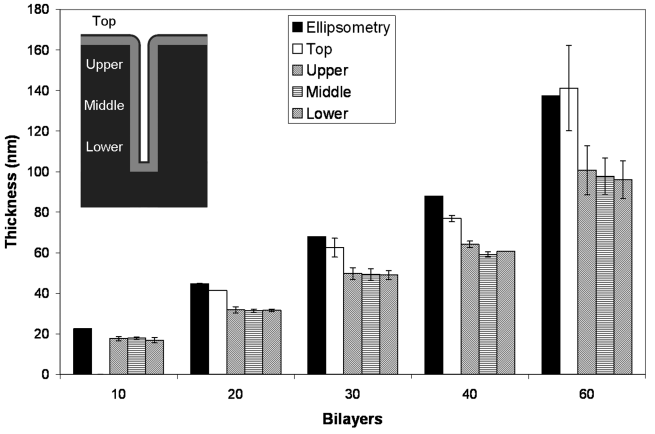

Figure 4. Comparison of dry state PEM thickness outside of and within a nanochannel for PAH/PSS multilayers deposited at pH 4.0 with 0.1 M added NaCl. The nanochannels had an initial gap size of 415 ± 41 nm. The black bars ("Ellipsometry") correspond to ellipsometry measurements on a flat silicon wafer. The white bars ("Top") correspond to SEM measurements of the unconfined PEM thickness on the top of the posts. The various striped bars ("Upper," "Middle," and "Lower") correspond to SEM measurements of the confined PEM thickness along the height of the nanochannel.

Figure 4. The data show that there is no systematic variation in the bilayer thickness with depth into the nanochannel, suggesting that deposition under these conditions is not limited by diffusion of the polyelectrolytes within the nanochannels.

On the contrary, the data in Figure 4 do indicate a measurable difference between the multilayer thickness inside (upper, middle, lower) and outside (top) the nanochannel. The SEM measurements on the outside of the channels agree with ellipsometric characterization of dry PEMs on flat silicon control substrates which were coated using LbL under the same conditions as the nanochannel arrays. Various salt concentrations were also used in an attempt to determine how the bilayer thickness changes with increasing ionic strength in the polymer solutions used in the LbL assembly process. The data for 0.1 and 0.25 M NaCl for both nanochannels and flat substrates are shown in Figure 5. The fitted slopes of these growth curves, which represent the bilayer thickness, are presented along with additional results for 0.5 M, 1 M NaCl, and for no added salt in Table 1. These data raise a few interesting

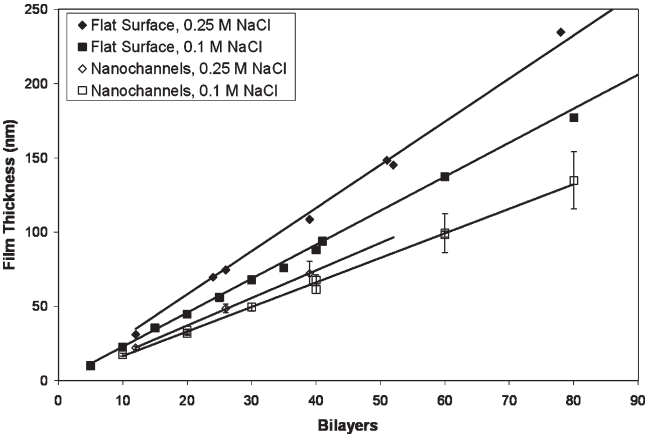

Figure 5. Comparison of dry state PEM thickness in channels and on a flat surface at different ionic strengths for PAH/PSS multilayers deposited at pH 4.0. The filled diamonds and filled squares represent ellipsometry measurements of film thickness on a flat surface for 0.25 and 0.1 M respectively. The open diamonds and open squares are the corresponding SEM measurements of film thickness within the channels.

Table 1. Dry State Bilayer Thicknesses Obtained by LbL Assembly of PAH and PSS at Various Salt Concentrations[a]

salt concentration (M)	flat surface bilayer thickness (nm)	nanochannel bilayer thickness (nm)	flat surface to nanochannel thickness ratio
0	0.576	0.313	1.84
0.1	2.31	1.69	1.38
0.25	2.94	1.86	1.58
0.5	3.78	2.76	1.37
1.0	5.14		

[a] The flat silicon substrate data are from spectroscopic ellipsometry measurements and the nanochannel data were obtained using SEM. The nanochannel bilayer thickness at 1.0 M NaCl is not included since these PEMs showed extreme roughness and poor film uniformity.

points. First, both nanochannel and flat surface substrates show linear growth with all best fit lines going nearly through the origin. Second, the bilayer thickness in all cases is proportional to the square root of the ionic strength and is therefore inversely proportional to the Debye length (see plotted data in Figure S4 of the Supporting Information) as observed by others.[54−56] Lastly, the data show that deposition within the nanochannels results in bilayer thicknesses similar to, but clearly lower than those obtained on flat surfaces. This result is contrary to previous reports where significantly larger[35,44] or significantly smaller[36] deposition thicknesses per cycle of processing were reported within confined geometries.

One explanation for the somewhat lower than expected bilayer thickness in the nanochannels is the depletion of unadsorbed polyelectrolyte within the channel. Depletion of polyelectrolytes confined between two charged surfaces has been predicted by Böhmer et al. using self-consistent field simulations.[55] Suppose that we start with a negatively charged surface which is dipped into a polycation solution. In the planar case, the positively charged polymer molecules are readily adsorbed at the surface creating a concentration gradient and a resultant driving force which causes a higher flux of polycation molecules toward the surface. This continues until the surface charge reverses and increases to a point at which further adsorption is impossible due to electrostatic repulsion. In the nanochannel case, an additional step is added, namely diffusion of polymer molecules from the bulk into the confined channel. According to Böhmer et al., for small gaps at low salt concentrations,

which result in low charge screening, the adsorption of polyanions onto an initially positively charged surface results in a negative potential throughout the channel. This potential reduces the flux of polyanions into the channel, lowering the polyanion concentration within the channel thereby hindering further adsorption.[55] In contrast to the planar case, adsorption in this case is limited by transport into the channel, explaining our observation of somewhat thin, but uniform multilayers along the length of the channel. This surface charge-induced depletion effect is attenuated by the presence of ions in the solution due to electrostatic screening; thus at the elevated ionic strengths we have employed (the gap is about 250 times larger than the Debye length), we see fairly similar, though slightly lower bilayer thicknesses due to confinement. In the absence of added salt, we would expect to observe a more dramatic effect. In fact we observe that for PAH/PSS deposited at pH 4 without additional salt where the gap is only 8 times larger than the Debye length, the PEM thickness after 50 bilayers is only about 16 nm in a 230 nm channel. In contrast we measured a film thickness of 33 nm on a flat silicon surface. At these conditions, Böhmer et al. do predict significant depletion throughout the channel. Though not conclusive, due to the fact that the very low multilayer thicknesses involved make these measurements more sensitive to error, this result indicates that the discrepancy between confined and unconfined LbL assembly is more pronounced at lower salt concentrations as shown in the last column of Table 1. Additionally, Figure 4 also shows increasing discrepancy between film thickness outside and within the channel as the film thickness increases and the gap thickness decreases in agreement with this hypothesis.

It should be noted that the polyelectrolytes used in this study are polydisperse; similar polyelectrolytes have a polydispersity index of over 6.[57] As a result, coils significantly larger than the averages quoted above are involved and this could account for lower bilayer thicknesses within the channel. It has been established that although polyelectrolytes in extended configurations result in a film whose bilayer thickness is molecular weight-independent, those in coiled, loopy conformations such as we would expect in a solution of moderate ionic strength do show molecular weight-dependent bilayer thicknesses.[58] Thus, if the top surface is in equilibrium with a higher average molecular weight ensemble than the confined surface due to the physical exclusion of high molecular weight polyelectrolytes, this may account for the thickness discrepancy. This effect may also be due to steric hindrance which starts to affect diffusion rates even for polymers whose radius of gyration is well below the size of a pore or channel.[25] In LbL, our aim is to approach equilibrium and the fact that we see uniform thickness along the channel wall suggests that deposition cycles are sufficiently long for polymer to diffuse into the channel. The effect of steric hindrance may also be mitigated by the fact that, as Deen pointed out, the dynamic nature of a polymer coil can result in diffusion through pores which are much smaller than the radius of gyration.[59]

The uniformity and conformality of the PEM coating allows us not only to functionalize the surface of the nanochannels, but also to tune the nanochannel gap size, reducing it uniformly and systematically to a desired value, which is crucial for nanofluidic applications. An important metric for this technique is how small and uniform a gap size can be obtained by assembling multilayers in the nanochannels. We have been able to reduce the gap size (open width of nanochannel) from 222 to 11 nm after deposition of 50 bilayers of PAH/PSS at pH 4.0. Protrusions and occasional

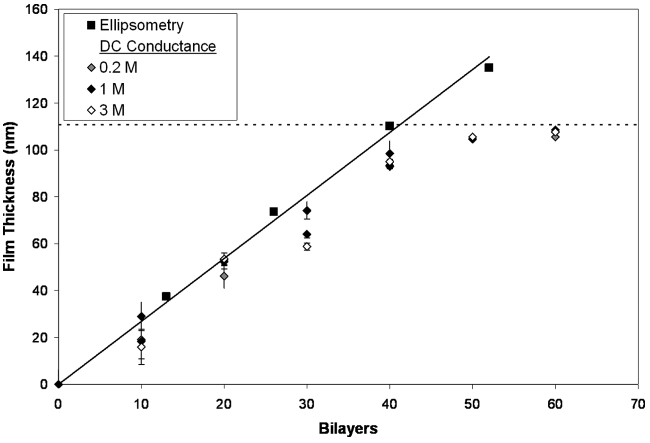

Figure 6. Comparison of wet state PAH/PSS (pH 4.0, 0.1 M NaCl) multilayer thickness measurements obtained by two different methods: measured on a flat silicon surface under 1 M KCl using ellipsometry (solid squares) and calculated from dc conductance measurements using 0.2 M KCl (gray diamonds), 1 M KCl (black diamonds), and 3 M KCl (white diamonds) as the electrolyte. The dashed line represents the maximum possible film thickness within the nanochannel.

bridging of polymer between the sidewalls of the nanochannel were sometimes observed when the dry state gap size (measured via SEM) was below 150 nm and when no salt was added. The frequency of observation of these defects increases as the gap size becomes smaller (see Figure S5 in the Supporting Information). When these defects are present, most of the channel is unaffected so that the performance of a nanochannel device would be largely unaltered. We believe that this effect may be caused by incomplete rinsing or by contamination and that possible remedies include performing LbL assembly using a high-flow filtration process[33] instead of the diffusion-dependent dipping method.

Wet-State Film Thickness Measurement by Dc Conductance. The dc conductance measurement was used to determine the wet-state thickness of a PEM film in a nanochannel as described in the Experimental Section. The high-aspect-ratio nanochannels have the advantage of high throughput (large open volume), but as a result the electrical resistance of the nanochannels is comparable to or even significantly smaller than that of the microchannels, especially for nanochannels with large gap sizes. This fact raises the potential for significant errors in calculating the nanochannel gap size using eq 6. In order to improve the measurement resolution, we significantly reduced the resistance of the microchannels by employing large, pyramid-shaped microchannels, as shown in Figure 2a. The dc conductances of channel circuits (S_{13}, S_{24}, S_{12}, and S_{34}) were determined by fitting the slopes of the $I-V$ curves. Figure 6 shows the swollen thickness of hydrated PAH/PSS multilayers deposited at pH 4.0 and a NaCl concentration of 0.1 M in nanochannels, calculated from conductance measurements using eq 8, and on a flat surface measured by *in situ* ellipsometry as a function of the number of bilayers.

First, we see that the dc conductance measurements were performed with 0.2, 1, and 3 M KCl. These experiments were used to further verify our assumption of bulk behavior and negligible surface charge effects on nanochannel conductance. Stein and co-workers studied surface-charge-governed transport in nanofluidic channels[49] and reported that at low salt concentrations, the electrical conductances of nanochannels saturated, becoming independent of both concentration and channel height. For 70 nm deep planar nanochannels, this transition occurred around 0.01 M;[49] therefore more concentrated electrolyte solutions were used

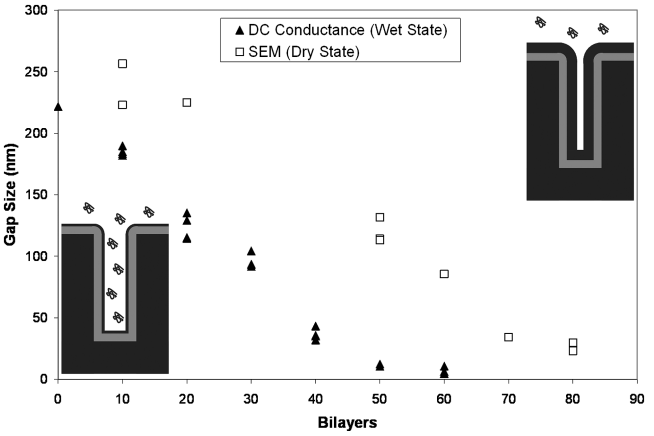

Figure 7. Nanochannel gap size as a function of the amount of PAH/PSS deposited at pH 4.0 and 0.1 M NaCl measured using two different methods: dc conductance (black triangles) and SEM (white squares). Note that dc conductance is a measure of wet state thickness while SEM is a measure of dry state thickness. The initial gap thickness for the dc conductance device was about 220 nm while the open arrays used for SEM had initial gap thicknesses ranging from 300 to 325 nm.

in our experiments. As expected, the nanochannel conductance varied linearly with salt concentration in all cases (data not shown) and no significant differences were observed for the swollen thicknesses calculated from the measurements using the three different electrolyte solutions. These observations confirm the validity of our treatment of the PEM-coated nanochannels as idealized, inert channels at the high salt concentrations used here.

Second, it has been well-established that some polyelectrolyte multilayers can swell significantly when immersed in salt solution[60−62] (see Figure S1, Supporting Information). Thus, the wet-state thickness of a PEM film, which is measured by dc conductance, can vary significantly from its dry-state thickness, which is measured by SEM or ellipsometry. We used ellipsometry to measure both the dry state and wet state thicknesses of a PEM film on a flat silicon wafer. The percent (%) swelling of the multilayers deposited on a flat substrate, defined as (wet thickness − dry thickness)/dry thickness ×100%, was about 26%. This value agrees well with the value of 22% for PAH/PSS reported previously.[61]

Third, at high numbers of bilayer processing steps, the wet-state thickness of the LbL films on the nanochannel walls asymptotes to a constant value of about 105 nm at which point the gap size of the nanochannels is only about 11 nm. In Figure 7, we recast these data to show the dependence of the gap size on the number of deposited bilayers and compare them with our results for SEM (see Figure S6 (Supporting Information) for more complete SEM data). We can see that in both cases we observe a deviation from linearity at low gap size, at about 11 nm for the conductance measurement and at about 34 nm for SEM. It should be noted that since dc conductance is a measure of the wet state thickness and SEM is a measure of the dry state thickness, we would expect the SEM data to asymptote at a higher value. These values are on the same length scale as the radius of gyration of the polyelectrolytes, and thus we would expect to see size-based exclusion of the polymer molecules, resulting in a failure to sustain LbL assembly within the channels.

Lastly, we can see that the dc conductance-derived data in Figure 6 compare favorably with the *in situ* ellipsometry measurements performed with 1 M KCl and, like the SEM data, show slightly lower bilayer thicknesses. The data were not directly compared with the SEM data due to the fact that SEM data were always taken in the dry state while conductance data were always taken in the wet state. See the Supporting Information for a direct comparison (Figure S7). The wet state results show that electrical resistance measurements are an efficient, nondestructive alternative for measuring the channel gap thickness in PEM-coated nanochannel arrays.

Conclusion

In this work, we have conformally coated high aspect ratio nanofluidic devices using LbL assembly of PAH and PSS. This procedure has been used to systematically narrow the wet-state nanochannel gap from 222 nm down to about 11 nm, at which point further LbL processing does not lead to any appreciable narrowing of the gap for the PAH/PSS polyelectrolyte pair used in this study. The deposited film thickness in the nanochannel did not show any significant depth dependence, demonstrating that this technique is suitable for building hybrid nanofluidic systems. We have shown that prior to the onset of size-based exclusion that occurs for very small gaps, the bilayer thicknesses are lower than those obtained for a flat surface. The magnitude of this effect is more pronounced at lower salt concentrations, but is always less than a factor of 2. This phenomenon was rationalized by the charge-based exclusion of polyelectrolytes between two closely spaced charged surfaces. Simple conductivity measurements were developed to calculate the gap thickness of nanochannels embedded within a microfluidic device. These conductivity measurements have been validated by comparison with SEM and ellipsometry results, and at the high ionic strengths used in this study the results are independent of the KCl electrolyte concentration.

The results obtained here point toward experiments to investigate in more detail how the confined bilayer thickness depends on the nature of the materials being deposited as well as the ionic strength of the LbL assembly solutions and the coated nanochannel gap thickness. Of particular interest is the question of whether or not charged nanoparticles can be deposited in a controlled manner using the nanochannel-confined LbL assembly process described above. A detailed study of polymer/nanoparticle and all nanoparticle systems is currently underway in our laboratory.

Acknowledgment. This work was supported in part by the MRSEC Program of the National Science Foundation under award numbers DMR-0819762 and DMR-0213282 and by the Intelligent Microsystems Center (IMC) of KIST, Korea. The authors would also like to thank the NSF Graduate Research Fellowship Program for funding; the Microsystems Technology Laboratories (MTL), the Center for Materials Science and Engineering (CMSE), and the Institute for Soldier Nanotechnologies (ISN) for use of the fabrication and characterization facilities; and Shreerang Chhatre for helpful discussions regarding this manuscript.

Supporting Information Available: Figures showing comparison of ellipsometry and profilometry data, representative $I-V$ plot from dc conductance measurement, schematic of nanochannel geometry, plot of Table 1 showing the variation of film thickness with ionic strength, SEM of coating showing bridging, plot of gap thickness as a function of deposited bilayers for a variety of initial gaps, and comparison of SEM and dc conductance data. This material is available free of charge via the Internet at http://pubs.acs.org.

References and Notes

(1) Decher, G.; Schlenoff, J. B., *Multilayer Thin Films*. Wiley-VCH: Weinheim, Germany, 2003.

(2) Lee, D.; Rubner, M. F.; Cohen, R. E. *Nano Lett*. **2006**, *6*, 2305–2312.
(3) Wu, Z.; Lee, D.; Rubner, M. F.; Cohen, R. E. *Small* **2007**, *3*, 1445–1451.
(4) Wu, Z.; Walish, J.; Nolte, A.; Zhai, L.; Cohen, R. E.; Rubner, M. F. *Adv. Mater*. **2006**, *18*, 2699–2702.
(5) Podsiadlo, P.; Sui, L.; Elkasabi, Y.; Burgardt, P.; Lee, J.; Miryala, A.; Kusumaatmaja, W.; Carman, M. R.; Shtein, M.; Kieffer, J.; Lahann, J.; Kotov, N. A. *Langmuir* **2007**, *23*, 7901–7906.
(6) Hiller, J. A.; Mendelsohn, J. D.; Rubner, M. F. *Nat. Mater*. **2002**, *1*, 59–63.
(7) Bravo, J.; Zhai, L.; Wu, Z.; Cohen, R. E.; Rubner, M. F. *Langmuir* **2007**, *23*, 7293–7298.
(8) Zhai, L.; Berg, M. C.; Cebeci, F. C.; Kim, Y.; Milwid, J. M.; Rubner, M. F.; Cohen, R. E. *Nano Lett*. **2006**, *6*, 1213–1217.
(9) Zhai, L.; Cebeci, F. C.; Cohen, R. E.; Rubner, M. F. *Nano Lett*. **2004**, *4*, 1349–1353.
(10) Cebeci, F. C.; Wu, Z.; Zhai, L.; Cohen, R. E.; Rubner, M. F. *Langmuir* **2006**, *22*, 2856–2862.
(11) Li, Z.; Lee, D.; Sheng, X.; Cohen, R. E.; Rubner, M. F. *Langmuir* **2006**, *22*, 9820–9823.
(12) Lee, D.; Cohen, R. E.; Rubner, M. F. *Langmuir* **2005**, *21*, 9651–9659.
(13) Lichter, J. A.; Rubner, M. F. *Langmuir* **2009**, *25*, 7686–7694.
(14) Chua, P.-H.; Neoh, K.-G.; Kang, E.-T.; Wang, W. *Biomaterials* **2008**, *29*, 1412–1421.
(15) Malcher, M.; Volodkin, D.; Heurtault, B.; Andrè, P.; Schaaf, P.; Möhwald, H.; Voegel, J.-C.; Sokolowski, A.; Ball, V.; Boulmedais, F.; Frisch, B. *Langmuir* **2008**, *24*, 10209–10215.
(16) Boulmedais, F.; Frisch, B.; Etienne, O.; Lavalle, P.; Picart, C.; Ogier, J.; Voegel, J. C.; Schaaf, P.; Egles, C. *Biomaterials* **2004**, *25*, 2003–2011.
(17) Swiston, A. J.; Cheng, C.; Um, S. H.; Irvine, D. J.; Cohen, R. E.; Rubner, M. F. *Nano Lett*. **2008**, *8*, 4446–4453.
(18) Mendelsohn, J. D.; Yang, S. Y.; Hiller, J. A.; Hochbaum, A. I.; Rubner, M. F. *Biomacromolecules* **2003**, *4*, 96–106.
(19) Thompson, M. T.; Berg, M. C.; Tobias, I. S.; Rubner, M. F.; Van Vliet, K. J. *Biomaterials* **2005**, *26*, 6836–6845.
(20) Lee, D.; Cohen, R. E.; Rubner, M. F. *Langmuir* **2007**, *23*, 123–129.
(21) Zhang, L.; Li, Y.; Sun, J.; Shen, J. *Langmuir* **2008**, *24*, 10851–10857.
(22) Barker, S. L. R.; Ross, D.; Tarlov, M. J.; Gaitan, M.; Locascio, L. E. *Anal. Chem*. **2000**, *72*, 5925–5929.
(23) Saleh, O. A.; Sohn, L. L. *Proc. Natl. Acad. Sci. U. S. A*. **2003**, *100*, 820–824.
(24) Sohn, L. L.; Saleh, O. A.; Facer, G. R.; Beavis, A. J.; Allan, R. S.; Notterman, D. A. *Proc. Natl. Acad. Sci. U.S.A*. **2000**, *97*, 10687–10690.
(25) Fu, J.; Yoo, J.; Han, J. *Phys. Rev. Lett*. **2006**, *97*, 018103.
(26) Han, J.; Craighead, H. G. *Science* **2000**, *288*, 1026–1029.
(27) Fu, J.; Mao, P.; Han, J. *Appl. Phys. Lett*. **2005**, *87*, 263902–3.
(28) Fu, J.; Schoch, R. B.; Stevens, A. L.; Tannenbaum, S. R.; Han, J. *Nat. Nanotechnol*. **2007**, *2*, 121–128.
(29) Llopis, S. L.; Osiri, J.; Soper, S. A. *Electrophoresis* **2007**, *28*, 984–993.
(30) Mao, P.; Han, J. *Lab Chip* **2009**, *9*, 586–591.
(31) Wang, Y. C.; Stevens, A. L.; Han, J. *Anal. Chem*. **2005**, *77*, 4293–4299.
(32) Wang, Y.; Angelatos, A. S.; Caruso, F. *Chem. Mater*. **2008**, *20*, 848–858.
(33) Ai, S.; Lu, G.; He, Q.; Li, J. *J. Am. Chem. Soc*. **2003**, *125*, 11140–11141.
(34) Hou, S.; Harrell, C. C.; Trofin, L.; Kohli, P.; Martin, C. R. *J. Am. Chem. Soc*. **2004**, *126*, 5674–5675.
(35) Lee, D.; Nolte, A. J.; Kunz, A. L.; Rubner, M. F.; Cohen, R. E. *J. Am. Chem. Soc*. **2006**, *128*, 8521–8529.
(36) Arsenault, A. C.; Halfyard, J.; Wang, Z.; Kitaev, V.; Ozin, G. A.; Manners, I.; Mihi, A.; Miguez, H. *Langmuir* **2005**, *21*, 499–503.
(37) Krogman, K. C.; Lowery, J. L.; Zacharia, N. S.; Rutledge, G. C.; Hammond, P. T. *Nat. Mater*. **2009**, *8*, 512–518.
(38) Sui, Z.; Schlenoff, J. B. *Langmuir* **2003**, *19*, 7829–7831.
(39) Graul, T. W.; Schlenoff, J. B. *Anal. Chem*. **1999**, *71*, 4007–4013.
(40) Liu, Y.; Xue, Y.; Ji, J.; Chen, X.; Kong, J.; Yang, P.; Girault, H. H.; Liu, B. *Mol. Cell. Proteomics* **2007**, *6*, 1428–1436.
(41) Wang, Y.; Angelatos, A. S.; Dunstan, D. E.; Caruso, F. *Macromolecules* **2007**, *40*, 7594–7600.
(42) Angelatos, A. S.; Wang, Y.; Caruso, F. *Langmuir* **2008**, *24*, 4224–4230.
(43) Barker, S. L. R.; Tarlov, M. J.; Canavan, H.; Hickman, J. J.; Locascio, L. E. *Anal. Chem*. **2000**, *72*, 4899–4903.
(44) Alem, H.; Blondeau, F.; Glinel, K.; Demoustier-Champagne, S.; Jonas, A. M. *Macromolecules* **2007**, *40*, 3366–3372.
(45) Wang, Y.; Yu, A.; Caruso, F. *Angew. Chem., Int. Ed*. **2005**, *44*, 2888–2892.
(46) Wang, Y.; Caruso, F. *Chem. Mater*. **2006**, *18*, 4089–4100.
(47) Nolte, A. J.; Rubner, M. F.; Cohen, R. E. *Macromolecules* **2005**, *38*, 5367–5370.
(48) Schoch, R. B.; Han, J.; Renaud, P. *Rev. Mod. Phys*. **2008**, *80*, 839.
(49) Stein, D.; Kruithof, M.; Dekker, C. *Phys. Rev. Lett*. **2004**, *93*, 035901.
(50) Durstock, M. F.; Rubner, M. F. *Langmuir* **2001**, *17*, 7865–7872.
(51) Hirose, E.; Iwamoto, Y.; Norisuye, T. *Macromolecules* **1999**, *32*, 8629–8634.
(52) Brandrup, J.; Immergut, E. H., *Polymer Handbook*, 3rd ed.; Wiley: New York, 1989.
(53) Borochov, N.; Eisenberg, H. *Macromolecules* **2002**, *27*, 1440–1445.
(54) Baur, J. W. Ph.D. Thesis, Department of Materials Science and Engineering, Massachusetts Institute of Technology: Cambridge, MA, **1997**.
(55) Böhmer, M. R.; Evers, O. A.; Scheutjens, J. M. H. M. *Macromolecules* **1990**, *23*, 2288–2301.
(56) Cosgrove, T.; Obey, T. M.; Vincent, B. *J. Colloid Interface Sci*. **1986**, *111*, 409–418.
(57) Nolte, A. J.; Takane, N.; Hindman, E.; Gaynor, W.; Rubner, M. F.; Cohen, R. E. *Macromolecules* **2007**, *40*, 5479–5486.
(58) Shiratori, S. S.; Rubner, M. F. *Macromolecules* **2000**, *33*, 4213–4219.
(59) Deen, W. M. *AIChE J*. **1987**, *33*, 1409–1425.
(60) Hiller, J.; Rubner, M. F. *Macromolecules* **2003**, *36*, 4078–4083.
(61) Dubas, S. T.; Schlenoff, J. B. *Langmuir* **2001**, *17*, 7725–7727.
(62) Itano, K.; Choi, J.; Rubner, M. F. *Macromolecules* **2005**, *38*, 3450–3460.